npj | climate and atmospheric science

www.nature.com/npjclimatsci

ARTICLE OPEN

Check for updates

Changes in hail hazard across Australia: 1979–2021

Timothy H. Raupach[1,2]✉, Joshua S. Soderholm[3], Robert A. Warren[3] and Steven C. Sherwood[1,2]

Hail damage is a leading cause of insured losses in Australia, but changes in this hazard have not been robustly quantified. Here, we provide a continental-scale analysis of changes in hail hazard in Australia. A hail proxy applied to reanalysis data shows that from 1979–2021 annual hail-prone days decreased over much of Australia but increased in some heavily populated areas. For example, the annual number of hail-prone days increased by ~40% around Sydney and Perth, the largest cities on Australia's east and west coasts, respectively. Changes in atmospheric instability have driven the trends. Radar observations, while covering shorter time spans and a more limited area than the reanalysis, corroborate the broad pattern of results. This study shows consistent hail-frequency trends in radar indicators and atmospheric environments and demonstrates substantial increases in hail frequency in major Australian cities where hail impacts are most significant.

npj Climate and Atmospheric Science (2023)6:143 ; https://doi.org/10.1038/s41612-023-00454-8

INTRODUCTION

Hail is a major meteorological hazard in Australia, with single hail events capable of inflicting insured losses of over AUD $1b[1–3]. The Australian cities of Sydney, Brisbane and Canberra have all been affected by billion-dollar hailstorm events (normalised to 2017 dollars)[4], and from 2014 to 2021, the seven most costly hailstorms in Australia caused a total of AUD $7.4b in insured losses[3]. Anthropogenic climate change is expected to affect hailstorms, yet the exact nature of the changes remains stubbornly difficult to quantify and therefore highly uncertain in Australia and across the globe[5]. Australia is sparsely populated, and hail reports and radar observations of hailstorms are generally restricted to more populated regions[1,6], frustrating efforts to quantify past and expected future changes to hailstorms across the whole Australian landmass. Here, we combine a hail proxy with radar observations to provide detailed continental estimates of recent trends in hail-hazard frequency in Australia.

Hail occurs under particular conditions inside of thunderstorms. Not any storm will do: hail forms only when there is sufficient supercooled liquid water to freeze onto the outside of embryo ice particles, when there is a strong enough updraught to support the growing embryos and when the storm structure allows the embryos to remain in the hail-growth region for sufficient time to grow larger than 5 mm in diameter[7]. Wind shear (changes in horizontal wind speed and direction with height) influences storm structure and the trajectory of a growing hailstone within the storm, so it is an important influence on the size the hailstone can attain[8,9]. Wind shear is required for the formation of supercell storms, the type of thunderstorm most likely to produce damaging hail[10]. To reach the ground as hail, hailstones must be sufficiently large to survive melting as they fall through warmer air[11].

Based on these physical processes, there are, globally, three main expected effects of anthropogenic climate change on hailstorms[5]. First, atmospheric instability is expected to increase owing to increased saturation deficit in a warmer atmosphere[12], affecting storm initiation and leading to stronger updraughts that can produce larger hailstones. Second, the melting-level height, at which the wet-bulb temperature is 0 °C, is higher in a warmer atmosphere[13]. A higher melting-level height implies more melting of falling hailstones and allows only the larger hailstones to survive, eliminating surface hail[14] or increasing the mean hailstone size[15]. Third, overall vertical wind shear is expected to decrease[10]. A decrease in wind shear would normally be expected to reduce hailstorm intensity[10], but the situation is complicated because local changes in wind shear may differ at times when hailstorms occur[16,17]. Combining these offsetting factors, the broad expectation is that under climate change, surface hail may become less frequent due to increased melt but more severe owing to increased hailstone size at the ground[5]. However, observations and simulated projections show that this expectation does not hold everywhere, with strong geographical inhomogeneity in climate responses and the resulting effects on hailstorms[5].

Hailstorms are notoriously difficult to observe and model because they are small-scale and relatively rare phenomena[5]. In locations where no ground observations are available, environment-based hail proxies are often the best tool for estimating the probability of hail occurrence[5,10]. Such hail proxies use an "ingredients-based" approach[18] to take information on the large-scale atmospheric environment and, from it, estimate the probability of hail reaching the surface: they commonly use some combination of measures of instability and wind shear[6,19,20]. A summary of such hail proxies, and other proxy ingredients and methods that have been used, is given in previous work[20]. A difficulty faced by all ingredients-based methods is that environments considered hail-prone often do not produce hail[21], and initiation mechanisms, which are crucial for actual storm formation in a storm-prone environment[22], are difficult to include in proxies[5]. The use of additional data, such as those provided by radar, can help to verify proxy information[23]. Few proxies have been trained for use in Australia[6,20,24–26], where there are latitudinal differences in atmospheric conditions that lead to hailstorm formation[20]. The proxy we use here[20] takes these differences into account and is designed specifically to detect hailstorms, whereas previous instability–shear proxies used in Australia were trained using the broader category of severe storms that may also include tornadoes or damaging straight-line winds[6,27,28]. This recently developed proxy better captures geographic variations than earlier proxies[20].

[1]Climate Change Research Centre, UNSW Sydney, Mathews Building Level 4, The University of New South Wales, Sydney 2051 NSW, Australia. [2]ARC Centre of Excellence for Climate Extremes, UNSW Sydney, Sydney, Australia. [3]Science and Innovation Group, Bureau of Meteorology, Melbourne, Australia. ✉email: timothy.h.raupach@gmail.com

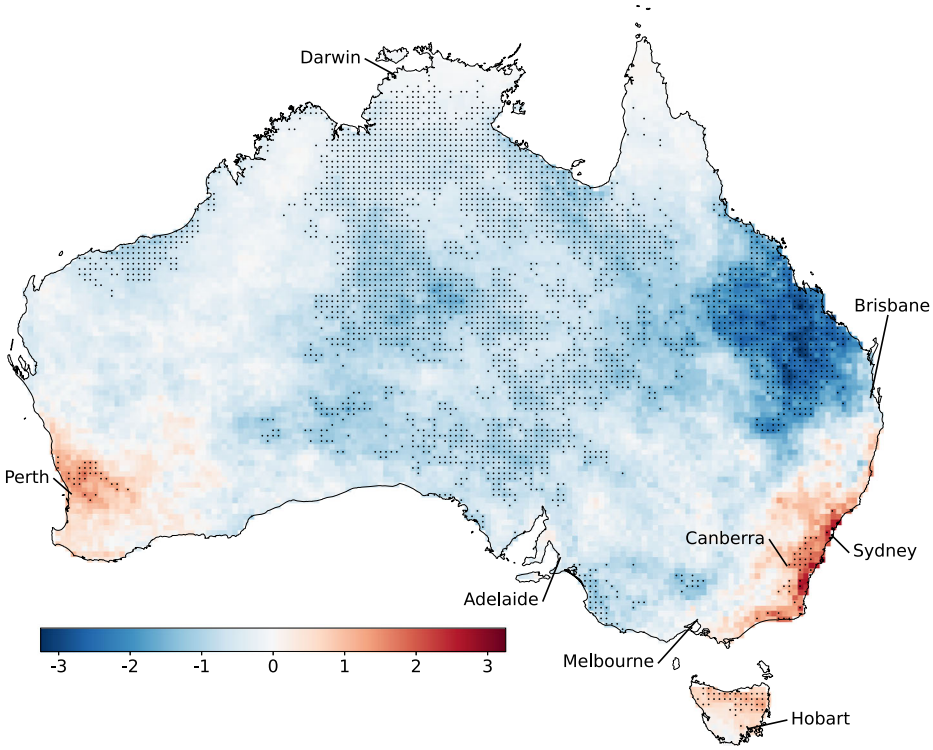

Fig. 1 Trends in annual hail-prone days [days decade^{-1}] 1979–2021. Stippling shows points where the linear trend is statistically significant at a 5% significance level and where no significant autocorrelation is detected by the Durbin–Watson test[53]. The locations of Australia's state and territory capital cities are indicated. Relative trends are shown in Supplementary Fig. 4.

The Australian regions most prone to hail are the continent's central east coast from north of Brisbane to south of Sydney[1,29–31], and the Canberra region[32], with indications of increased hail probability in southeast Western Australia[30]. Environmental proxy-based studies of severe storms often identify Australia's northwest as a particularly active region[19,20,31,33], as do satellite-based detections of hail signatures[29,34], but the degree to which these signals correspond to hail at the surface is uncertain[1,20,30,31,33].

Studies of historical or projected hail trends for Australia are few and have focused on the southeast of the continent[5]. A hail-loss model for two eastern locations found no statistically significant climate change effects in a scenario with doubled CO_2 levels[24]. A comparison of simulations for 1980–2000 and 2040–2060 showed decreases in hail frequency and no change in severity at two point locations in the southeast[25], although the conclusions on frequency were based on projected decreases in atmospheric instability that are contradicted by more recent analyses[35,36]. Hail reports for Sydney show a reduction in annual hail frequency in 1989–2002 compared to 1953–1988, though the more recent period is relatively short and contained a predominance of El Niño events whose impact on hail is uncertain[37]. Hail reports can also contain non-meteorological biases that complicate trend analyses[1,6]. For the broader category of severe storms that may include hail, a proxy[6] applied to simulations for 2079–2099 showed increases in severe-storm environment occurrences in Australia's east and north compared to 1980–2000[35], and global analyses show projected end-of-century increases for Australia's north and east[27]. Projections exploring responses to global temperature increases show increases in severe-storm-favourable conditions for most of Australia, with statistically significant trends, particularly in the northwest and southeast under larger (2–3 °C) temperature increases[28].

Here, we show a continental-scale analysis of the frequency of days with hail-prone environmental conditions and days on which radars detected hail signatures for Australia, providing hail-specific trend information for the past four decades with high-resolution and large spatial coverage. To do so, we applied a proxy specifically designed to detect hail-favourable conditions in Australia[20] to more than 40 years of reanalysis data and compared these results to observations from the Australian radar archive. For study details, see the "Methods" and Supplementary Information. Our work addresses how hail potential has changed in Australia over the last four decades overall, by season, and by city, providing information on changes in hail hazard in many regions where there was previously little guide. Additionally, we show that changes in atmospheric instability are the primary driver of the observed trends in hail-prone conditions.

RESULTS

Trends in hail-prone days

Figures 1 and 2 show trends in annual hail-prone days for the continent and zoomed in to selected cities, respectively (Supplementary Fig. 1 shows a map of the domain, while climatologies of hail-prone days are shown in Supplementary Figs. 2 and 3). Over most of Australia, the number of hail-prone days per year has decreased over the last four decades, with particular decreases over the mid-north of the country's east coast. There are, however, statistically significant increases in annual hail-prone days on the southern parts of the east and west coasts, which cover several major Australian cities. Relative changes in cities in which increases were detected are up to ~10% per decade around Sydney, Perth and Canberra, and up to ~20% per decade around Hobart. Decreases were detected around Darwin and Adelaide, and the trends around Brisbane and Melbourne are not statistically significant.

Seasonal trends in hail-prone days across all of Australia are shown in Fig. 3, and relative seasonal trends in hail-prone days over capital cities are shown in Supplementary Fig. 6. There are clear differences between the seasons. Most notably, there are

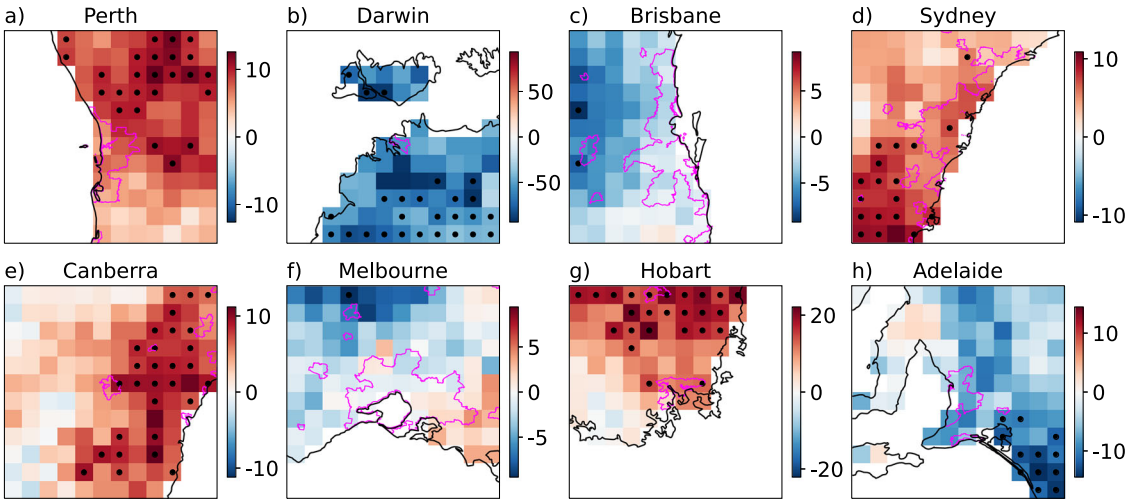

Fig. 2 Relative trends in annual hail-prone days around cities, 1979–2021. Relative trends per decade are shown as a percentage of mean annual hail-prone days at each point, for the regions around Perth (**a**), Darwin (**b**), Brisbane (**c**), Sydney (**d**), Canberra (**e**), Melbourne (**f**), Hobart (**g**), and Adelaide (**h**). Stippling is defined as in Fig. 1. Fuchsia lines show the boundaries of "significant urban areas"[55]. Note the sub-plots have different scales.

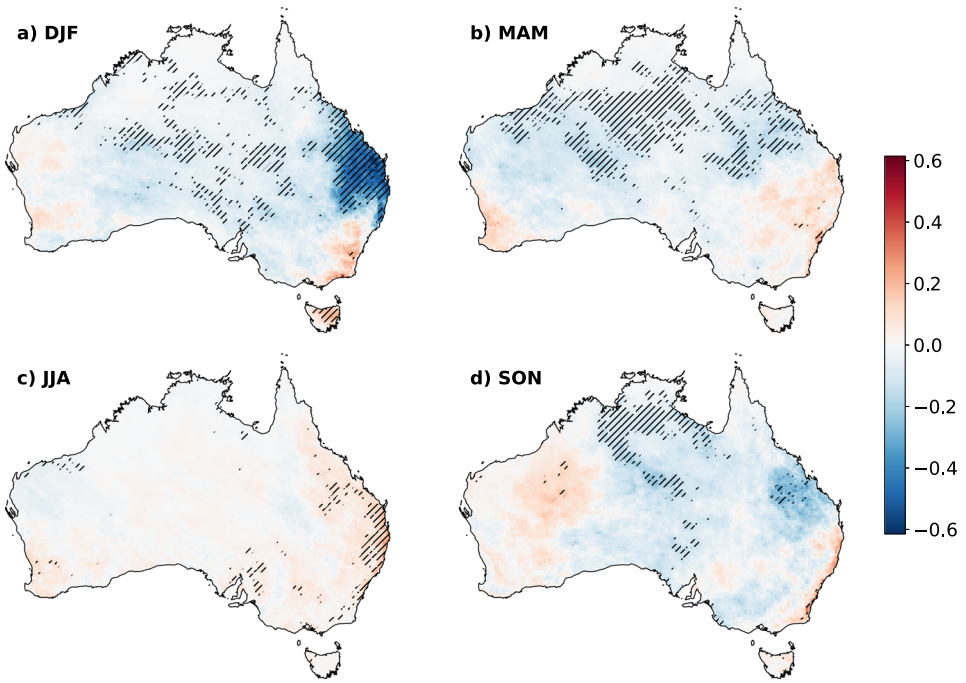

Fig. 3 Trends in hail-prone days [days decade^{-1}] per season, March 1979–May 2022. DJF (**a**) stands for December-January-February, MAM (**b**) for March-April-May, JJA (**c**) for June-July-August, and SON (**d**) for September-October-November. Hatching is defined as for stippling in Fig. 1. Relative seasonal trends are shown in Supplementary Fig. 5.

strong decreases in hail-prone day occurrence on Australia's northeast coast in summer but increases in the same region in winter. Areas showing increases in annual hail-prone day occurrence generally show increases across all seasons. Of the capital cities, Brisbane is notable for showing decreases in summer hail-prone days but increases in winter, whereas the Adelaide region shows statistically significant trends only in winter. Around most of these cities, the trend signal is stronger and more consistent in winter than in the other seasons.

Comparison with radar data

Proxy performance was analysed using radar data as a reference (see Supplementary Figs. 7 and 8). The false alarm ratio was high, as is expected with ingredients-based methods[20]. Overall, however, the proxy performed well in terms of identifying, as hail prone, days on which hail signatures were detected by radar. In Australia's north, the proxy probability of detection was low compared to radar detections. However, we note that the radar-based hail proxy detects possible hail only above the melting layer, which is high in the tropics, and there are uncertainties in whether hail aloft reaches the ground in these regions[1,20,30,31,33]. As such, it is likely that radars overestimate hail occurrence in these regions.

Figure 4 shows a comparison between trends derived from radar and proxy data for the three longest radar time series in each of six regions. Time-series plots are shown in Supplementary Figs. 9 and 10. The radar time series are less than half the length of

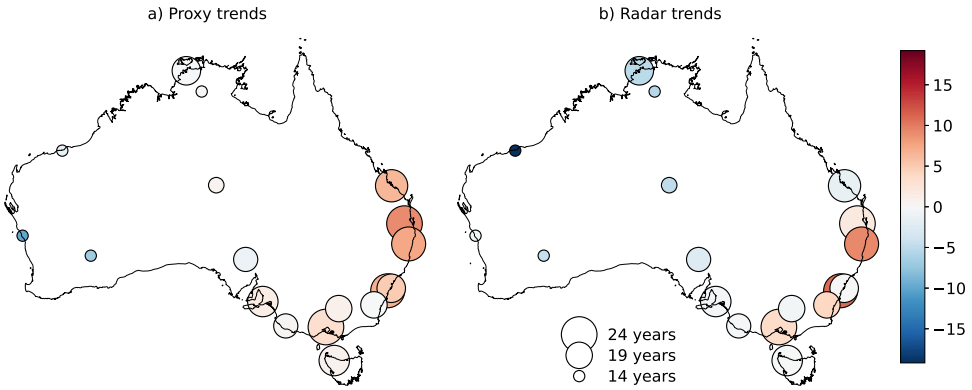

Fig. 4 Proxy and radar trend comparison. Trends on proxy (**a**) and radar (**b**) data are in days decade^{-1}. Points are sized by the number of years in the time series at each radar site. At each location, the same time periods and spatial points were used for both proxy and radar trends. See Supplementary Figs. 10 and 11 for time series for each site and a map of radar locations, respectively.

the reanalysis time series, and the trends compared are therefore often not statistically significant. The magnitude (and, in some cases, the sign) of trends differ between radar and proxy-based results in some locations, reflecting the large inter-annual variability in hail-prone environments. At Gladstone, the northernmost radar site on the east coast of Australia, the proxy-derived trend over the radar time period is increasing while the radar-derived trend is slightly decreasing. This area is subject to large inter-seasonal variability in trends (Fig. 3), which may make the overall trend sensitive to sampling effects. Nonetheless, the proxy and radar results both show increasing hail frequency on Australia's southeast coast and decreasing or near-constant hail frequency in the north, and time-series results show agreement in radar and proxy fluctuations.

At most of the sites in Fig. 4, trends in the proportions of proxy-derived hail-prone days that also recorded radar-detected hail are not statistically significant and have small slopes (see Supplementary Fig. 12). At some sites, the trends are skewed by the low number of hail environments detected by the proxy. The results indicate that since 2000 the proportion of hail-prone environments that result in hail has increased at Grafton, Wollongong, and Melbourne, all in Australia's southeast. The proportion has decreased in Gladstone (northeast) and Woomera (central south). These strongest changes have the same sign as the corresponding radar trends on hail days, indicating that the radar trends in these locations are stronger than the proxy trends. However, these results should be interpreted with caution owing to the short lengths of the radar time series.

Drivers of observed changes

Figure 5 shows relative trends in annual means of hail-proxy ingredients. Corresponding absolute trends are shown in Supplementary Fig. 13. Trends in annual means differ from trends in annual extreme values (Supplementary Fig. 14). Variables related to atmospheric instability (convective available potential energy (CAPE), the lifted index[38], and 700 to 500 hPa lapse rate) show trends towards more stable environments in the north, centre, and northeast of Australia, and more unstable environments in the southeast and southwest, which correspond to the observed changes in hail-prone day occurrence. Temperature-related indices (temperature at 500 hPa and melting-level height) show increases across the whole country, with changes in the melting-level height of a similar magnitude to global-mean changes previously reported[13]. Reductions in wind shear across the mid-north of Australia correspond with reducing hail-prone day occurrence.

Figure 6 shows the effects of individual ingredients on trends in hail-prone days by showing the differences made by applying the hail proxy to data in which one of the ingredients was detrended by removing the trend in its annual mean. Changes in instability made the largest contribution to the trends in annual hail-prone days. The increasing trends over Australia's southeast and southwest and decreases over the north were primarily explained by instability changes, while wind shear played a relatively minor role. Since instability trends over the southeast and southwest are strongest for extreme values of instability (Supplementary Fig. 14), we surmise that the trends in annual hail days in these locations are driven by changes in extreme instability values. Supplementary Figs. 15 and 16 show trends in selected percentiles of proxy ingredients by season. In northern and central-eastern Australia, extreme (99th percentile) CAPE has decreased in summer but increased in winter, which helps explain the seasonal differences in hail-proxy trends in Brisbane.

DISCUSSION

In this study, we used a hail proxy applied to reanalysis data and radar detections of hail signatures to examine trends in the frequency of hail-prone environments across all of Australia for the last four decades. Over this period, the frequency of hail-prone environments has decreased in most of Australia but increased in some of the most populated regions. Areas in which we show increases in hail-prone environments include regions of horticultural production that may be susceptible to hail damage[39]. These results are a reminder that hailstorm changes in a warming atmosphere are far from geographically universal[5]. They show the importance of local-scale effects and changes in atmospheric circulations that mean resulting differences in hail occurrence can differ from more thermodynamically based expectations[5]. These changes are primarily driven by changes in extreme atmospheric instability. It has previously been noted that decreases in 95th percentile values of summer CAPE in northern Australia are some of the largest decreases globally in the 1979–2019 ERA5 archive[40].

Our results, which are specifically for hailstorms, can be compared to those from studies looking at broader severe-storm environments that may or may not include hail. Changes in seasonal thunderstorm-environment frequencies based on reanalyses show spatial patterns similar to our proxy-derived hail-specific trends, with the exception that they do not show the increasing signal we observe in southwestern Australia[32]. Sub-hourly extreme rainfall measured by radar is increasing in Sydney[41], which aligns with the increasing trends we observe in instability in this region. Global trends in severe-storm environments from ERA5 show statistically significant decreases in environments over Australia's northeast, regions of statistically non-significant increases over the southeast and southwest, and statistically non-significant increases over some tropical regions[40]. Our results for hail environments broadly agree with these findings.

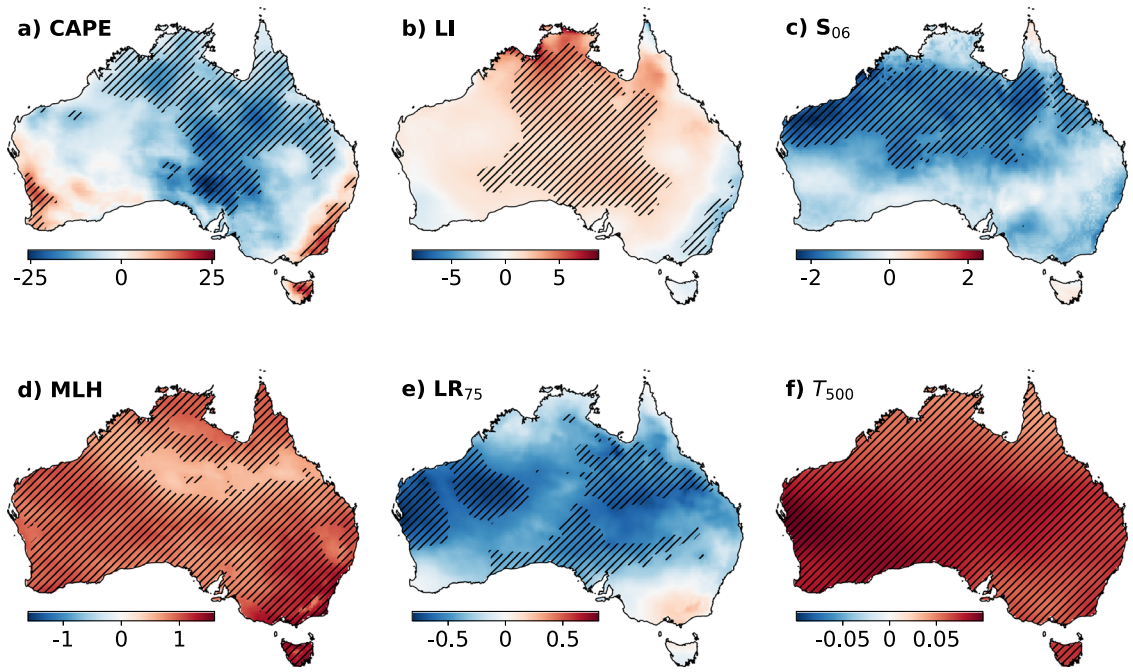

Fig. 5 Relative trends in annual means of hail-proxy ingredients, 1979–2021. CAPE (**a**) is mixed-layer convective available potential energy, LI (**b**) is the lifted index, S_{06} (**c**) is the 0–6 km bulk vertical wind shear, MLH (**d**) is melting-level height, LR_{75} (**e**) is the 700–500 hPa lapse rate, and T_{500} (**f**) is the temperature at 500 hPa. CAPE and LI were calculated using a well-mixed parcel over the lowest 100 hPa, and MLH was calculated using wet-bulb temperature. Trends are shown as percentages of the average annual mean at each point. Hatching is defined as for stippling in Fig. 1.

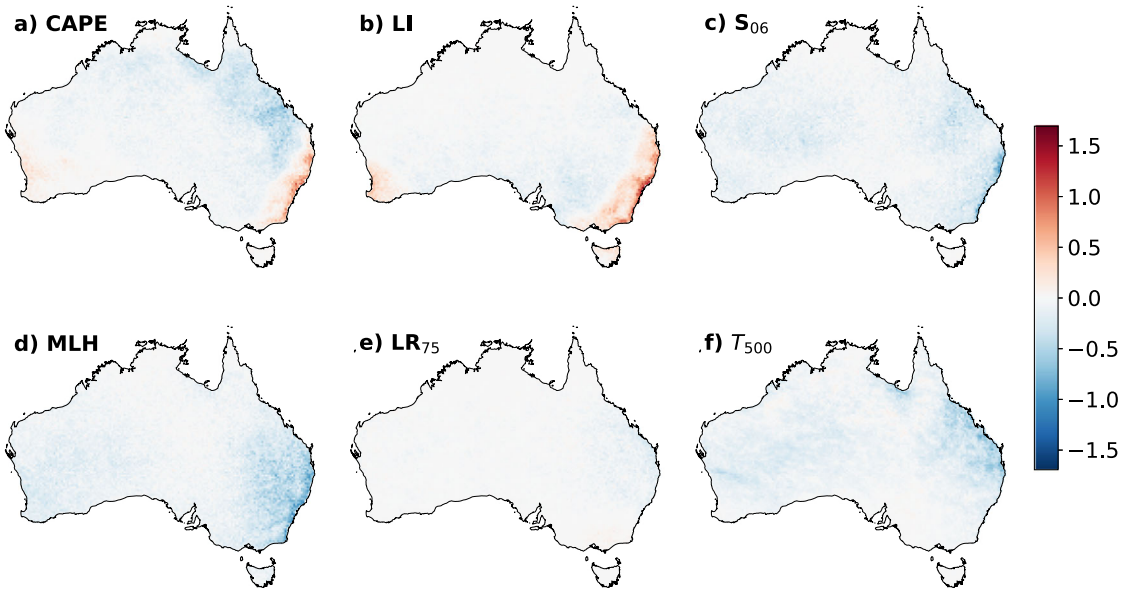

Fig. 6 Differences made by detrending individual ingredients. In each plot, the trend in the mean of one proxy ingredient, shown in the top left corner, was removed before the hail proxy was applied, while the other ingredients were left unchanged. Ingredient panels (**a**–**f**) are arranged as in Fig. 5. Values show the trend with all fields unaltered minus the trend with the selected ingredient detrended, in days decade^{-1}.

We note that past trends from ERA5 and rawinsonde data generally agree for S_{06} but paint a complex picture for the 95th percentile of CAPE, with rawinsonde data for Australia at 00 and 12 UTC generally showing increasing trends in contrast to trends from ERA5[40]. Rawinsonde data are spatially and temporally limited and are subject to their own uncertainties[40], yet these differences merit further investigation. While ERA5-derived convective parameters have been found to be reliable for Europe and North America[42], no comprehensive evaluation has been performed for Australia. Nevertheless, the pattern of our reanalysis-based trend results is corroborated by the similar pattern in radar trends.

While ERA5 shows CAPE has decreased across the north and centre of Australia over the last four decades, end-of-century projections for this region generally show extreme CAPE increasing[28,43] and wind shear decreasing[28,35], though not all studies agree on the spatial coverage of changes. Projected increases in CAPE are generally explained by thermodynamic changes[28,35], such as increased saturation deficit[12]. However, recent CAPE

changes vary regionally[40] and may not resemble longer-term forced changes, so they are not explained by planetary-scale mechanisms like large-scale warming alone but rather are influenced by regional factors that require further study. It is important to note that examining trends in any hail ingredient in isolation is not sufficient to understand trends in hail environments, owing to strong offsetting effects and interactions between ingredients[5,35].

This study does not explicitly address changes in hail severity or hailstone size. Increases in hail size are associated with wider and stronger updraughts and more-organised severe storms, which correspond to increases in both atmospheric instability and wind shear[9]. Increased melting can lead to a shift toward larger mean hailstone size when there is sufficient hail generation, because small hailstones melt completely and leave only larger hail[5]. We have shown that generally in Australia wind shear has decreased and melting-level height has increased, which would be expected to reduce hail severity through decreased storm organisation and increased hailstone melting, respectively. In the southeast and southwest, where instability shows increasing trends, hail severity would be expected to also increase, owing to a combination of increased hail generation and updraught strength and increased melting of small hailstones meaning that surface hail is more likely to be larger. However, the situation is complicated because increasing CAPE does not always increase hail size, with storm structure playing a critical role[9].

Convective initiation is difficult to quantify and can be affected by changes in large-scale dynamics, mesoscale processes, or convective inhibition[35,44]. Here, our treatment of initiation is limited to reporting on trends in the proportion of proxy-derived hail-prone environments that result in radar-detected hail, which show modest increases in some southeastern locations. Owing to relatively short radar records, we can not conclusively determine whether the percentage of hail-prone environments that lead to radar-detected hail has changed over the whole ERA5 archive. However, ERA5 convective precipitation can serve as a proxy for convective initiation, albeit with high uncertainty[40]. Changes in convective precipitation (1979–2019) indicate that convective initiation has decreased across the eastern half of Australia and increased in the southwest, but the changes are generally not statistically significant in regions where we find increases in annual hail-prone days[40]. To examine the effects of climate change on hailstorms in more detail, future work should include process-based understanding and high-resolution projections of future scenarios in which these uncertainties can be better resolved[5].

METHODS

Study region

The study region is the continent of Australia. We focus on eight $1.5 \times 1.5°$ domains of interest centred on the state and territory capital cities. The study region and city domains of interest are shown in Supplementary Fig. 1.

Data

Reanalysis data were European Centre for Medium-range Weather Forecasts (ECMWF) reanalysis 5 [ERA5][45] data on pressure levels[46] at 3, 6, and 9 UTC every day from January 1979 to June 2022. These times were selected to cover the most storm-prone hours in the diurnal cycle[1,47]. We analysed data from 1979 because ERA5 analysis quality for the southern hemisphere is much improved by the addition of satellite data from 1979[48]. As in the work in which the proxy was trained[20], we consider that ERA5 data interpolated to pressure levels provide convective parameters with sufficient accuracy for this analysis. Rare ERA5 profiles containing negative values of specific humidity (<0.01% of total points) were excluded from the analyses. Radar data were Level 2 data from the Australian Unified Radar Archive[49], which are provided on a 1 km grid with a maximum range of 150 km from the radar and include the severe hail index (SHI)[50]. We note that Australia's radar network is diverse, has been updated over time, and has used scanning strategies that are not always constant[2]. Confidence in the radar data is generally lower in remote or rural areas, where radars use older hardware, and higher in more populated areas.

Data processing

The proxy of Raupach et al.[20] was applied to ERA5 data with convective parameters calculated as in the proxy description[20]. To estimate whether hail was observed in radar data, we converted SHI to Maximum Expected Size of Hail (MESH)[50]. While MESH has limited skill for quantitative hail sizing, it can skillfully discriminate hail and no-hail events[2,51]. For simplicity, we used a standard threshold of 21 mm[51] for all considered radars to detect hail of any size. This threshold was previously used for a climatology of hail in southeast Queensland[52], while a study focused on large hail associated with property damage in Sydney and Brisbane used a threshold of 32 mm^2. Radar data with a sampling interval of 5–10 min were first aggregated to daily resolution by finding all pixels that recorded MESH >21 mm at any point between 3 and 9 UTC each day. To remove MESH values potentially caused by clutter, a speckle filter was applied to keep only hail detections (SHI > 0) encompassing more than 9 contiguous pixels. To remove days on which hardware failures occurred, any day on which the domain-maximum value of MESH increased by more than 75 mm between two consecutive timesteps was considered a fault day and was removed. If two fault days were separated by less than 7 days and the intervening days all had maximum MESH values over 75 mm, the intervening days were considered faulty and also removed. Aggregated daily data were regridded to a 0.25° latitude and longitude grid to match the ERA5 data, using a maximum operator such that each grid point indicated whether any of its subpoints exceeded the MESH threshold. We masked the regridded data to land points using the ERA5 land–sea mask. For comparison between radar and proxy trends, we subset each dataset to points where both proxy and radar information was available, then found the maximum over all these points; the result was, for each radar site, a time series of proxy-derived hail-prone days and days on which hail was detected by radar for matching points. To ensure adequate temporal coverage, for each radar site, any year on which less than 250 days were covered was removed from the analysis.

Trend analysis

We found trends using least-squares linear regression on data aggregated by year or by season. The type of aggregation depended on the variable: for the hail proxy and radar data, we found the mean number of hail-prone days per year or season, then normalised by multiplying by 365 for annual hail-prone days or 90 for seasonal hail-prone days. For hail-proxy ingredients, we aggregated temporally by finding the mean or percentile. An example of the regression process for a single point is shown in Supplementary Fig. 17. To test for autocorrelation, we used the Durbin–Watson test[53] and looked for significant negative or positive serial correlation. Using tables, the lower bound for the test statistic at a 5% significance level and for 45 samples is 1.48[53]. For trends on reanalysis data, we therefore counted the Durbin–Watson test statistic d as showing significant serial correlation if $d < 1.48$ or $(4 - d) < 1.48$ [53]. For simplicity and ease of interpretation, we used linear regression even though residuals may not always be perfectly normal[54].

DATA AVAILABILITY

The data used in this work are available in the National Computational Infrastructure (NCI) data catalogue (identifiers are https://doi.org/10.25914/5fb115b82e2ba for ERA5 data and https://doi.org/10.25914/JJWZ-0F13 for radar data). The results contain modified Copernicus Climate Change Service information 2022. Neither the European Commission nor ECMWF is responsible for any use that may be made of the Copernicus information or data it contains. Shapefiles for the significant urban areas used in figures in this paper are from the Australian Bureau of Statistics and are available under CC-BY-4.0 at https://www.abs.gov.au/statistics/standards/australian-statistical-geography-standard-asgs-edition-3/jul2021-jun2026/access-and-downloads/digital-boundary-files.

CODE AVAILABILITY

The underlying code for this study is available in a Zenodo repository (https://doi.org/10.5281/zenodo.8231600) and uses library `xarray_parcel` by T.H.R. (https://doi.org/10.5281/zenodo.8088497) for calculation of convective indices.

Received: 10 April 2023; Accepted: 11 August 2023;
Published online: 19 September 2023

REFERENCES

1. Allen, J. T. & Allen, E. R. A review of severe thunderstorms in Australia. *Atmos. Res.* **178–179**, 347–366 (2016).
2. Warren, R. A. et al. Radar-based climatology of damaging hailstorms in Brisbane and Sydney, Australia. *Q. J. Roy. Meteor. Soc.* **146**, 505–530 (2020).
3. Lawrence, J. et al. Australasia. *Climate Change 2022: Impacts, Adaptation and Vulnerability* (eds Pörtner, H. O. et al.) Contribution of Working Group II to the Sixth Assessment Report of the Intergovernmental Panel on Climate Change, 1581–1688 (Cambridge University Press, 2022).
4. Insurance Council of Australia. *Historical Catastrophe Data—February 2023*. https://insurancecouncil.com.au/industry-members/data-hub/ (Insurance Council of Australia, 2022).
5. Raupach, T. H. et al. The effects of climate change on hailstorms. *Nat. Rev. Earth Environ.* **2**, 213–226 (2021).
6. Allen, J. T., Karoly, D. J. & Mills, G. A. A severe thunderstorm climatology for Australia and associated thunderstorm environments. *Aust. Meteorol. Ocean. J.* **61**, 143 (2011).
7. Knight, C. A. & Knight, N. C. Hailstorms. *Severe Convective Storms* (ed. Doswell, C. A.) 223–254 (American Meteorological Society, 2001).
8. Dennis, E. J. & Kumjian, M. R. The impact of vertical wind shear on hail growth in simulated supercells. *J. Atmos. Sci.* **74**, 641–663 (2017).
9. Lin, Y. & Kumjian, M. R. Influences of CAPE on hail production in simulated supercell storms. *J. Atmos. Sci.* **79**, 179–204 (2022).
10. Brooks, H. E. Severe thunderstorms and climate change. *Atmos. Res.* **123**, 129–138 (2013).
11. Fraile, R., Castro, A., López, L., Sánchez, J. L. & Palencia, C. The influence of melting on hailstone size distribution. *Atmos. Res.* **67–68**, 203–213 (2003).
12. Seeley, J. T. & Romps, D. M. Why does tropical convective available potential energy (CAPE) increase with warming? *Geophys. Res. Lett.* **42**, 10429–10437 (2015).
13. Prein, A. F. & Heymsfield, A. J. Increased melting level height impacts surface precipitation phase and intensity. *Nat. Clim. Change* **10**, 771–776 (2020).
14. Mahoney, K., Alexander, M. A., Thompson, G., Barsugli, J. J. & Scott, J. D. Changes in hail and flood risk in high-resolution simulations over Colorado's mountains. *Nat. Clim. Change* **2**, 125–131 (2012).
15. Xie, B., Zhang, Q. & Wang, Y. Trends in hail in China during 1960–2005. *Geophys. Res. Lett.* **35**, L13801 (2008).
16. Diffenbaugh, N. S., Scherer, M. & Trapp, R. J. Robust increases in severe thunderstorm environments in response to greenhouse forcing. *Proc. Natl Acad. Sci. USA* **110**, 16361–16366 (2013).
17. Rädler, A. T., Groenemeijer, P. H., Faust, E., Sausen, R. & Púčik, T. Frequency of severe thunderstorms across Europe expected to increase in the 21st century due to rising instability. *NPJ Clim. Atmos. Sci.* **2**, 30 (2019).
18. Doswell, C. A., Brooks, H. E. & Maddox, R. A. Flash flood forecasting: an ingredients-based methodology. *Weather Forecast.* **11**, 560–581 (1996).
19. Brooks, H. E., Lee, J. W. & Craven, J. P. The spatial distribution of severe thunderstorm and tornado environments from global reanalysis data. *Atmos. Res.* **67–68**, 73–94 (2003).
20. Raupach, T. H., Soderholm, J., Protat, A. & Sherwood, S. C. An improved instability-shear hail proxy for Australia. *Mon. Weather Rev.* **151**, 545–567 (2023).
21. Tippett, M. K., Allen, J. T., Gensini, V. A. & Brooks, H. E. Climate and hazardous convective weather. *Curr. Clim. Change Rep.* **1**, 60–73 (2015).
22. Kottmeier, C. et al. Mechanisms initiating deep convection over complex terrain during COPS. *Meteorol. Z.* **17**, 931–948 (2008).
23. Tang, B. H., Gensini, V. A. & Homeyer, C. R. Trends in United States large hail environments and observations. *NPJ Clim. Atmos. Sci.* **2**, 45 (2019).
24. McMaster, H. J. The potential impact of global warming on hail losses to winter cereal crops in New South Wales. *Clim. Change* **43**, 455–476 (1999).
25. Niall, S. & Walsh, K. The impact of climate change on hailstorms in southeastern Australia. *Int. J. Climatol.* **25**, 1933–1952 (2005).
26. Allen, J. T., Karoly, D. J. & Walsh, K. J. Future Australian severe thunderstorm environments. Part I: A novel evaluation and climatology of convective parameters from two climate models for the late twentieth century. *J. Climate* **27**, 3827–3847 (2014).
27. Singh, M. S., Kuang, Z., Maloney, E. D., Hannah, W. M. & Wolding, B. O. Increasing potential for intense tropical and subtropical thunderstorms under global warming. *Proc. Natl Acad. Sci. USA* **114**, 11657–11662 (2017).
28. Lepore, C., Abernathey, R., Henderson, N., Allen, J. T. & Tippett, M. K. Future global convective environments in CMIP6 models. *Earth's Future* **9**, e2021EF002277 (2021).
29. Cecil, D. J. & Blankenship, C. B. Toward a global climatology of severe hailstorms as estimated by satellite passive microwave imagers. *J. Clim.* **25**, 687–703 (2012).
30. Bedka, K. M., Allen, J. T., Punge, H. J., Kunz, M. & Simanovic, D. A long-term overshooting convective cloud-top detection database over Australia derived from MTSAT Japanese Advanced Meteorological Imager observations. *J. Appl. Meteorol.* **57**, 937–951 (2018).
31. Prein, A. F. & Holland, G. J. Global estimates of damaging hail hazard. *Weather Clim. Extremes* **22**, 10–23 (2018).
32. Dowdy, A. J. Climatology of thunderstorms, convective rainfall and dry lightning environments in Australia. *Clim. Dyn.* **54**, 3041–3052 (2020).
33. Allen, J. T. & Karoly, D. J. A climatology of Australian severe thunderstorm environments 1979–2011: inter-annual variability and ENSO influence. *Int. J. Climatol.* **34**, 81–97 (2014).
34. Bang, S. D. & Cecil, D. J. Constructing a multifrequency passive microwave hail retrieval and climatology in the GPM domain. *J. Appl. Meteorol.* **58**, 1889–1904 (2019).
35. Allen, J. T., Karoly, D. J. & Walsh, K. J. Future Australian severe thunderstorm environments. Part II: The influence of a strongly warming climate on convective environments. *J. Clim.* **27**, 3848–3868 (2014).
36. Chen, J., Dai, A., Zhang, Y. & Rasmussen, K. L. Changes in convective available potential energy and convective inhibition under global warming. *J. Clim.* **33**, 2025–2050 (2020).
37. Schuster, S. S., Blong, R. J. & McAneney, K. J. Relationship between radar-derived hail kinetic energy and damage to insured buildings for severe hailstorms in eastern Australia. *Atmos. Res.* **81**, 215–235 (2006).
38. Galway, J. G. The lifted index as a predictor of latent instability. *Bull. Am. Meteorol. Soc.* **37**, 528–529 (1956).
39. Randall, L., Mobsby, D. & Addai, D. *Australia's Agricultural Industries Map 2020*. Asset name: pb_aaim9aa_20200825. https://doi.org/10.25814/5f323003195bc (ABARES, 2020).
40. Taszarek, M., Allen, J. T., Marchio, M. & Brooks, H. E. Global climatology and trends in convective environments from ERA5 and rawinsonde data. *NPJ Clim. Atmos. Sci.* **4**, 35 (2021).
41. Ayat, H., Evans, J. P., Sherwood, S. C. & Soderholm, J. Intensification of subhourly heavy rainfall. *Science* **378**, 655–659 (2022).
42. Taszarek, M. et al. Comparison of convective parameters derived from ERA5 and MERRA-2 with rawinsonde data over Europe and North America. *J. Clim.* **34**, 3211–3237 (2021).
43. Brown, A. & Dowdy, A. Severe convective wind environments and future projected changes in Australia. *J. Geophys. Res. Atmos.* **126**, E2021JD034633 (2021).
44. Taszarek, M., Allen, J. T., Brooks, H. E., Pilguj, N. & Czernecki, B. Differing trends in United States and European severe thunderstorm environments in a warming climate. *Bull. Am. Meteorol. Soc.* **102**, E296–E322 (2020).
45. Hersbach, H. et al. The ERA5 global reanalysis. *Q. J. Roy. Meteor. Soc.* **146**, 1999–2049 (2020).
46. Hersbach, H. et al. *ERA5 Hourly Data on Pressure Levels from 1979 to Present*. Copernicus Climate Change Service (C3S) Climate Data Store (CDS). https://doi.org/10.24381/cds.bd0915c6 (2018).
47. Dowdy, A. J., Soderholm, J., Brook, J., Brown, A. & McGowan, H. Quantifying hail and lightning risk factors using long-term observations around Australia. *J. Geophys. Res. Atmos.* **125**, 2020JD033101 (2020).
48. Bell, B. et al. The ERA5 global reanalysis: preliminary extension to 1950. *Q. J. Roy. Meteor. Soc.* **147**, 4186–4227 (2021).
49. Soderholm, J., Louf, V., Protat, A., Warren, R. & Brook, J. *AURA—Operational Radar Network Level 2 Archive*. https://doi.org/10.25914/JJWZ-0F13 (2022).

50. Witt, A. et al. An enhanced hail detection algorithm for the WSR-88D. *Weather Forecast.* **13**, 286–303 (1998).
51. Cintineo, J. L., Smith, T. M., Lakshmanan, V., Brooks, H. E. & Ortega, K. L. An objective high-resolution hail climatology of the contiguous United States. *Weather Forecast.* **27**, 1235–1248 (2012).
52. Soderholm, J. S. et al. An 18-year climatology of hailstorm trends and related drivers across southeast Queensland, Australia. *Q. J. Roy. Meteor. Soc.* **143**, 1123–1135 (2017).
53. Durbin, J. & Watson, G. S. Testing for serial correlation in least squares regression. II. *Biometrika* **38**, 159–177 (1951).
54. Knief, U. & Forstmeier, W. Violating the normality assumption may be the lesser of two evils. *Behav. Res. Methods* **53**, 2576–2590 (2021).
55. Australian Bureau of Statistics. *Australian Bureau of Statistics Jul 2021–Jun 2026, Significant Urban Areas.* https://www.abs.gov.au/statistics/standards/australian-statistical-geography-standard-asgs-edition-3/jul2021-jun2026/significant-urban-areas-urban-centres-and-localities-section-state/significant-urban-areas (2022).

ACKNOWLEDGEMENTS

This research was undertaken with the assistance of resources and services from the NCI, which is supported by the Australian Government. The authors thank Dr. Adrien Guyot and Dr. Valentin Louf for pre-submission reviews of the manuscript.

AUTHOR CONTRIBUTIONS

This study was designed and conducted by T.H.R. J.S.S. and R.A.W. provided advice on the use of radar data. All authors contributed to the experimental design and interpretation of results. T.H.R. drafted the manuscript, and all authors contributed to editing prior to submission.

COMPETING INTERESTS

The authors declare no competing interests.

ADDITIONAL INFORMATION

Supplementary information The online version contains supplementary material available at https://doi.org/10.1038/s41612-023-00454-8.

Correspondence and requests for materials should be addressed to Timothy H. Raupach.